Heliostat-field gain-scheduling control applied to a two-step solar hydrogen production plant

Lidia Roca[a,*], Alberto de la Calle[a], Luis J. Yebra[a],

[a] *CIEMAT - Plataforma Solar de Almería, Ctra. De Senés s/n 04200 Tabernas, Spain*

Abstract

This article describes a temperature control structure designed for the interior of a solar hydrogen reactor based on a two-step ferrite-redox technology. Until now, this temperature has been controlled by manual selection of the heliostats to be focused on the receiver targets. However, the strong system dependency on operating conditions suggests that the procedure be automated in order to ensure the desired setpoint change response. The aims are to maintain the desired temperatures and to make the setpoint switch as fast as possible, keeping plant conditions within the margins of safety. The scheme proposed includes a procedure for selecting the heliostats to be focused on the reactor by using a simple model of the solar field and a gain scheduling control system which changes the control tuning parameters to deal with the varying dynamics observed during the process. Real experiments show the promising results of this work.

Key words: Heliostat control, Gain scheduling, Thermochemical cycle, Hydrogen

*Corresponding author. Tel.:+34 950 387964; Fax: +34 950 365015

Email addresses: lidia.roca@psa.es (Lidia Roca), alberto.calle@psa.es (Alberto de la Calle), luis.yebra@psa.es (Luis J. Yebra)

1. Introduction

Hydrogen could soon replace fossil fuels as an energy resource in many applications [1] , and solar hydrogen production is today a promising line of research with high potential for meeting the future hydrogen demand in high solar irradiance areas. The main sustainable energies used for producing hydrogen are solar, hydro, ocean thermal, tidal, wind, biomass, geothermal and nuclear [2]. Regarding the solar source, the main solar thermochemical hydrogen production processes are thermochemical cycles, reforming, cracking and gasication [3, 4, 5]. strong interest in the use of concentrated solar thermochemical processes, there is much ongoing research in this area. Examples are new redox pairs, such as ferrites and aluminum spinels, for hydrogen production by thermochemical water splitting [6], hybrid sulfur thermochemical cycles [7], the use of parabolic trough collectors as reactors for producing hydrogen by methane steam reforming [8], dynamic models for reducing reradiation losses in a porous ceramic bed [9] and maintaining steady-state in a compound parabolic concentrator solar reactor system with a thermal storage system [10].

Although research now underway in two-step thermochemical water-splitting cycles promises to improve reactant efficiency and reactor design [11], few studies are focused on control strategies to optimize system production efficiency. Some examples of control applied to solar thermal hydrogen processes are given in [12, 13]. In [12], a non-linear first principles model was developed for a solar hydrogen reactor. This model is applied to solar thermal gasification of petcoke where the object of control is to ensure constant product

composition at the outlet (CO, CO_2, H_2). The control design combines a feedback controller with a feedforward block where the control signal is the reactant mass flow rate (petcoke with steam). [13] describes of a model for a two-step solar chemical cycle. This model includes the solar field, the reactors and hydrogen production. It also presents system control requirements, such as reaching the desired reactor temperature and keeping the solar ux distribution homogeneous.

The present paper proposes a control scheme for reaching the desired reaction temperature in the experimental solar hydrogen production plant described in [14]. The gain scheduling controller employed is widely used in the solar industry, e.g., for maintaining the desired heat transfer medium outlet temperature in distributed solar collector fields using the fluid flow rate as the manipulated variable [15]. Gain scheduling is used when changes in the process dynamics suggest to adapt the controller depending on the operating point. In solar collector fields, gain-scheduling can handle plant nonlinearities, by applying local linear models to design local linear controllers using various tuning techniques.

The gain scheduling controller presented in this paper deals with different system dynamics from which control tuning may be inferred depending on the temperature setpoint.

Hydrogen is produced in the Hydrosol II pilot plant installed in the SSPS solar tower at the CIEMAT-Plataforma Solar de Almería (PSA), Spain [16]. Two ferrite redox reactors perform parallel two-step processes, which, when sequentially switched, generate quasi-continuous hydrogen production.

Operation of central receiver systems such as this one, requieres a control

system which integrates heliostat aiming strategies for control of solar flux distribution control, heliostat offset correction and the process control for the particular application [17]. Artificial-vision systems using CCD cameras were used in [18] to maintain the temperature distribution on the receiver surface as uniform as possible. This solution reduces thermal gradients in the receiver and increases its lifetime. CCD cameras can also handle offset corrections, such as the one proposed in [19]. The images taken by the cameras are used as feedback to calculate the offset correction.

In the problem described in the present paper, the heliostats are focused on predefined receiver aiming points. These targets are changed manually depending on the concentrated solar power on the receiver. The automatic controller proposed uses the mean reactor temperature as feedback and selects the heliostats to be focused or taken out of focus. This is a major challenge to a solar energy system connected to a hydrogen production process because of the operating problems caused by solar variability.

The paper is organized as follows: Section 2 gives a brief overview of the plant. Section 3 describes the simple solar field model used for the gain-scheduled control structure explained in Section 4. Experimental results are reported and discussed in Section 5, and some conclusions are arrived at in Section 6.

2. System description

The solar hydrogen production pilot plant was erected at CIEMAT - PSA has a maximum power of 100 kW_{th} [16]. It consists of two reactors where hydrogen and oxygen production cycles are alternated for quasi-continuous

hydrogen production. The reactor absorbers are comprised of nine 0.146 m x 0.146 m x 0.06 m silicon carbide (SiC) honeycomb monoliths which are assembled in a single module. The SiC monoliths are used as the substrate for the oxides required for the reactions.

The reactors are installed half-way up the SSPS solar tower (see Fig. 1). Under typical conditions of 950 W/m^2, the total field capacity is 2.7 MWth and the peak flux is 2.5 MW/m^2. Approximately 99% of the power is collected in a 2.5 m-diameter circumference and 90% in a 1.8 m circumference. Since each reactor aperture is 0.5 m x 0.5 m, part of the solar flux is outside them. This also means that the power density inside the reactor is almost homogeneous.

The water-splitting step (1) is a exothermic reaction which takes place at an operating temperature of T_{gen} = 800℃. The thermal reduction step (2) is an endothermic reaction at an operating temperature of T_{reg}= 1200℃. Therefore, the power required by each is different. Both reactions require a gas atmosphere, that is, a mixture of nitrogen and steam in the generating cycle and nitrogen alone in the regenerating cycle. Nitrogen flows inside the reactor through the monolith channels where the reaction takes place, flushing the reaction products out.

$$MO_{reduced} + H_2O \rightarrow MO_{oxidized} + H_2 \tag{1}$$

$$MO_{oxidized} \rightarrow MO_{reduced} + \frac{1}{2}O_2 \tag{2}$$

Figure 1: The Hydrosol facility at CIEMAT-PSA

3. Simplified heliostat solar field model

Heliostats reflect solar radiation and concentrate it on the receiver apertures. Several algorithms have been proposed for calculating this solar flux concentration and its distribution on the central receiver. As explained in [20], there are two types of algorithms for calculating flux. The first are used in solar plant design software to maximize the solar energy collected, whereas the second are codes for evaluating the power reected by the heliostats onto the receiver. Since these algorithms are designed for a high degree of precision, such numerical models may be too complex, and require a computa-

tional effort too great to be used in real-time applications. Recent research has tried to minimize the time such algorithms require to solve the models without loss of accuracy. An example is a new ray-tracing program [21] that calculates the flux density distribution reducing the computation time compared to other Monte Carlo ray tracing approaches. Although heliostat field power density simulation is extremely accurate in a short computation time, the minimum computation time demonstrted is 13 s for a solar eld with 300 heliostats and therefore, control applications are limited to use of longer sampling times.

The solar field model used in this model is explained in [22]. It was developed for estimating the concentrated solar power in the Hydrosol facility receivers. To reduce the models complexity, the following simplications have been assumed:

- tracking errors are neglected,
- flux density on the receiver plane is homogeneous,
- slope, shading and blocking errors and optical efficiency are constants.

The concentrated solar power generated by the heliostat k, p_k, may be estimated as [22]:

$$p_k = I \cdot cos(\alpha_{ik}) \cdot A \cdot \beta \cdot (1 - \gamma) \tag{3}$$

and the total solar power concentrated on the receiver, P, is:

$$P = \sum_{k=1}^{n_t} p_k \cdot c_k \tag{4}$$

where n_t is the number of heliostats in the field, c_k is a boolean equal to 1 when heliostat k is focused and 0 otherwise, I is the direct solar irradiance, α_i

is incident angle of the solar vector on the heliostat plane, A is the heliostat mirror area, β is a parameter which includes optical efficiency, slope, tracking, shading and blocking errors, and γ is the atmospheric attenuation factor. The atmospheric attenuation factor is the one used in the MIRVAL code for a clear day [23]:

$$\gamma = 10^4 \cdot (67.9 + 1.176 \cdot S - 1.97 \cdot 10^4 \cdot S^2) \tag{5}$$

where S is the slant range in meters from the heliostat to the receiver, which must be less than one kilometer.

The incident angle depend on the Sun position, $\mathbf{U_s}$=(s_x, s_y, s_z), and on the azimuth and elevation angles of each heliostat, α_a, α_e,:

$$\alpha_{ik} = f(\mathbf{U_s}, \alpha_{ak}, \alpha_{ek}). \tag{6}$$

Since α_a and α_e depends on the coordinates of each heliostat, $\mathbf{U_h}$=(h_x, h_y, h_z), and the target receiver focus, $\mathbf{U_t}$=(t_x, t_y, t_z), α_i for heliostat k is:

$$\alpha_{ik} = f(\mathbf{U}_s, \mathbf{U}_{hk}, \mathbf{U}_t). \tag{7}$$

The algorithm proposed in [24] is used to determine the Sun coordinates. Since the model must be as simple as possible, it is assumed that there are no tracking errors and the ray reflected from the heliostat mirror center of mass reaches the target on the receiver.

Simulation results of this model can be found in [25, 22] and, as shown in [22], the numerical predictions show good agreement with measurement data.

As will be explained in Section 4.3, in the present paper this model is used to determine which heliostats must be focusing on the reactor to reach the desired temperature.

4. Control algorithm

The hydrogen production operation is a cycling process. As mentioned above, in the rst step of the cycle, the monoliths are reduced, releasing oxygen. In the next step, in which oxygen is taken from water, the material is oxidized and hydrogen is produced. In the regeneration process, the temperature in the reactor chamber must be 1200^{o}C, whereas for water-splitting it must be 800^{o}C. These temperatures may be controlled by the steam mass flow rate, feed preheater temperature or the number of heliostats focused. Since changes in the mass flow rate affect the reaction kinetics, and the effect of preheating is very slight, temperatures can only be controlled only with the heliostats [16] .

4.1. Manual control

As explained in [16], for solar flux in the two reactors to be different, two groups of heliostats are used. Each group is focused separately on a different receiver. The manual control strategy consists of identifying the mirrors that provide high-power (in ± 100℃) and low-power (± 20℃). The number of heliostats focused on the targets is modified manually to reach the desired temperature requirements.

Fig.2 shows the results of one of the experiments done during thermal monolith testing in the Hydrosol Facility. Cycles were reinitiated every 30 minutes by refocusing some of the heliostats. Reactor temperatures were maintained at 1200℃ and 800℃, and the target took from 6 to 13 minutes to cool down and over 15 minutes to heat up. Table 1 shows a summary of the main test parameters, where the settling time, T_{st}, is defined as the time

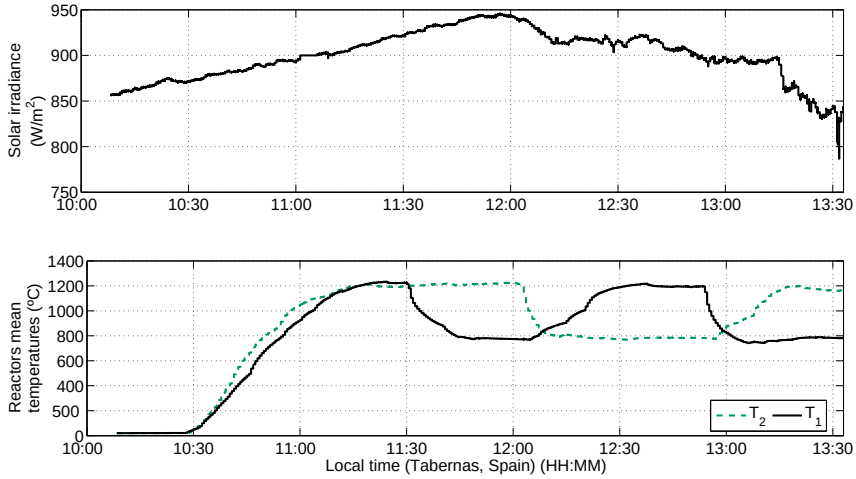

Figure 2: Test in the Hydrosol facility with manual heliostat control.

that elapses from the beginning of a setpoint step to the time the temperature takes to remain within a specified 5% margin of error. As observed, with manual control setpoint responses reach the desired temperature and maintain these temperatures quite well. Nevertheless, settling times and overshoots are in a wide range caused by process nonlinearities and disturbances. For example, at 11:30 T_{st} is 12.6 minutes and the temperature in reactor one is -773℃, whereas at 12:54 T_{st} drops to 6.6 minutes, but the temperature reaches 742℃.

Local time (HH:MM)	**Reactor**	**Step (℃)**	T_{st} **(min)**	**Overshoot (℃)**
10:28	1, 2	0-1200	42	32
11:30	1	1200-800	12.6	-27
12:03	2	1200-800	6	-31

12:04	1	800-1200	23.4	18
12:54	1	1200-800	6.6	-58
12:57	2	800-1200	18.6	-

Table 1: Main results of the manual heliostat control test.

4.2. Adaptive PI

As shown in Section 4.1, although manual control maintains the desired temperatures, the switching time (or T_{st} in this case) may exceed 23 minutes. Moreover, with manual control there is a wide range of settling times and overshoots.

Fig. 3 shows the scheme of an automatic controller proposed for achieving the desired temperatures in both reactors. This scheme is a typical hierarchical structure [26] in which control is divided into several subtasks each of which has a specific internal controller.

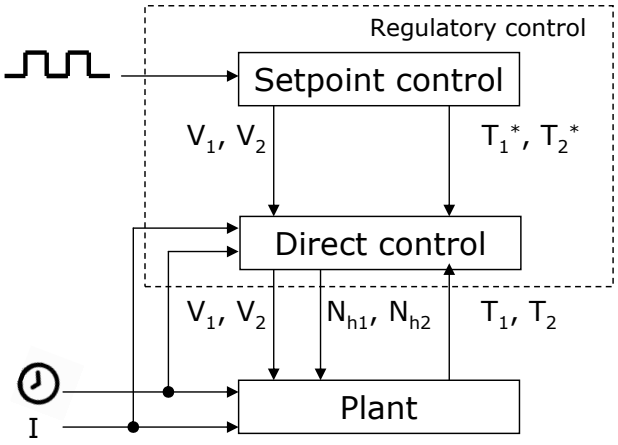

Figure 3: Proposed Hydrosol control scheme.

One of the goals of any industrial plant is to maximize production, making it economically viable. The general control therefore consists of several subtasks: to maintain safe plant operating conditions and keep the process from getting out of control, keep certain input and output variables within defined margins and maximize H_2 production.

In the multilayer control structure, the *direct control* layer is in charge of the safety tasks (maintaining safe plant operating conditions and keeping the process from getting out of control) and acts on the manipulated variables (the heliostats arrays) to reach the desired output values by selecting the heliostats to be focused on each target, $\mathbf{N}_{h1}$ and $\mathbf{N}_{h2}$, and on-ff valves V_1 and V_2, which switch reactor function (production or regeneration).

$\mathbf{N}_{h1}$ and $\mathbf{N}_{h2}$ are defined as boolean arrays:

$$\begin{aligned} \mathbf{N}_{h1} &\in \{c_{11}, c_{12}, ..., c_{1n_{t1}}\}/c_{1i} \in \{0,1\}, \quad i = 1...n_{t1} \\ \mathbf{N}_{h2} &\in \{c_{21}, c_{22}, ..., c_{2n_{t2}}\}/c_{2j} \in \{0,1\}, \quad j = 1...n_{t2} \end{aligned} \tag{8}$$

with n_{t1}, n_{t2} the maximum numbers of heliostats focused on receivers one and two, respectively. When $c_{ki} = 1$, heliostat i is focused on the target of receiver k.

The direct control layer uses temperatures T_1 and T_2 in the reactors, to reach desired temperatures. Assuming model- based control in this layer, solar irradiance, I, and time must also be known.

The *setpoint control* layer, which controls variables related to product quality, defines the two temperature references (one for production and the other regeneration) which are alternated in 30-minute cycles.

The regulatory control layer proposed is shown in Fig. 4. The *setpoint control* block calculates the two receiver temperature references. In the *Con-*

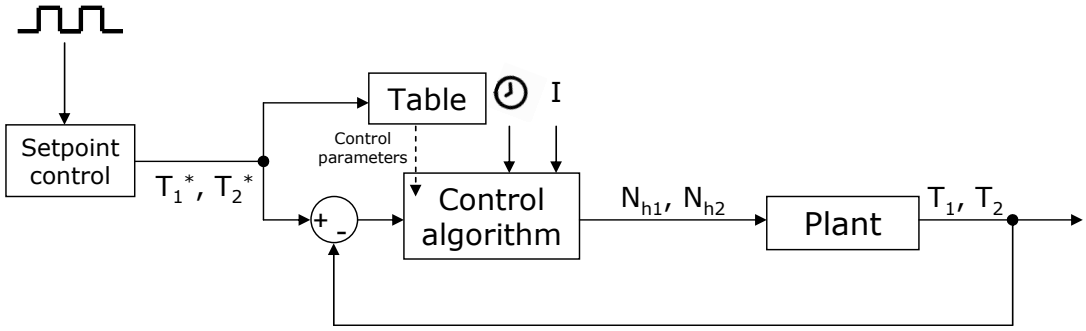

Figure 4: Regulatory layer.

trol algorithm block a PI control is used as feedback control to achieve the desired setpoint response. Although the purpose of the controller is for the temperature targets to be reached as fast as possible to make hydrogen production quasi-continuous, a critical issue in the water-splitting cycle is deactivation of the redox material in the high-temperature cyclic reaction [5]and the redox material may not exceed 1250℃ during regeneration [16]. Therefore, tuning is different for the two temperatures, faster for generation (800℃) and more conservative for regeneration (1200℃). So adaptive gain-scheduling [27, 28] is included in the PI controller to change the controller parameters according to the setpoint step. This technique has been used in industry for many years, mainly to effectively control systems in which the dynamics change with operating conditions. We used gain scheduling to achieve the desired setpoint responses. The *Table* block includes the gain scheduling where various predefined PI parameters (K_p and T_i), are selected

depending on which of the three setpoints is required, start-up, regeneration or water-splitting.

When the PI parameters are switched, the control signal, u, is kept continuous. Let us define the PI with a state space representation:

$$\dot{x}(t) = \quad A(t) \cdot x(t) + B(t) \cdot u(t) \tag{9}$$

$$y(t) = \quad C(t) \cdot x(t) + D(t) \cdot u(t), \tag{10}$$

where A is the state matrix, B the input matrix, C the output matrix, D the feed through matrix, x the state vector and y the output vector.

If a switch occurs at time t_{sw}, the output is maintained, $u(t_{sw} + T_s) = u(t_{sw})$, so the PI state must be calculated and propagated to the next sample time:

$$x(t_{sw}) = (y(t_{sw}) - D(t_{sw}) \cdot u(t_{sw}))/C(t_{sw}) \tag{11}$$

$$x(t_{sw} + T_s) = x(t_{sw}) \tag{12}$$

By resetting the PI state when there is a switch, control signal discontinuities are minimized. In this case, the control signal is the number of heliostats focused (n_{h1} for reactor one and n_{h2} for reactor two), but the control algorithm must also choose which heliostats are to be focused to generate arrays $\mathbf{N}_{h1}$ and $\mathbf{N}_{h2}$.

4.3. Focusing strategy

Although the control scheme shown in Fig. 4 is typical, the manipulated variables make the algorithm somewhat more complicated. As explained above, $\mathbf{N}_h$ is a vector of $\{0,1\}$, representing the heliostat that is focused. Moreover, the concentrated power reflected by each heliostat on the receiver

is different. Therefore, the controller not only has to calculate the number of heliostats to be focused, but also specify which ones. The following explanation is generalized to only one reactor.

Let us assume that each heliostat is characterized by an identifier numbered from 1 to n_t, where n_t is the total number of heliostats to be focused on a receiver. Then position k in $\mathbf{N}_h$ matches heliostat identifier k.

The model described in section 3 is used to evaluate the concentrated solar power of each heliostat assuming that all the heliostats are focused. As a first approximation, a simple algorithm is used to find the combination of heliostats to be focused.

First, a solar power arranged vector is calculated:

$$\mathbf{P}^{\xi} = \{p_1^{\xi}, p_2^{\xi}, ..., p_n^{\xi}\} / \quad p_i^{\xi} < p_{i+1}^{\xi}, \quad i = 1, ..., n_t - 1, \tag{13}$$

and the associated heliostat identifiers vector:

$$\mathbf{H} = \{h_1, h_2, ..., h_{n_t}\}, \tag{14}$$

where $h_i \in 1, ..., n_t$ is the heliostat identifier which produces p_i^{ξ}. For example, if heliostat k=3 is the one that contributes least to the concentrated solar power, h_1=3.

In addition, the output of the PI control is the number of heliostats, n_h, which must be added to reach the desired temperature references.

The algorithm proposed selects the heliostats starting from the smallest $\mathbf{P}^{\xi}$, using the control signal n_h found to evaluate the $\mathbf{N}_h$ array:

$$N_h(H(i)) = \left\{ \begin{array}{lll} 1 & if & i \leq n_h \\ 0 & if & i > n_h \end{array} \right\} \tag{15}$$

5. Results

This Section presents representative results of the solar field control for reaching the desired temperatures in one of the reactors. First the control algorithm was tested in simulations using the process model in [22], and then real experiments were carried out in the Hydrosol Plant.

5.1. Control simulation results

The rst step was to test the proposed control system using a model of the plant to evaluate its performance under different operating conditions. The model used must evaluate the production plant's thermal behavior, including the heliostat field and the processing plant. Therefore, the model described in [22] was used as the real plant. This nonlinear model based on physical principles was developed in the Modelica language and the low computational effort required makes it suitable for control purposes.

Processing plant model development minimized the number of equations while retaining essential principles. It is divided into four interconnected submodels (Fig. 5). The source submodel provides the reaction submodel with a constant mass flow rate, the composition of which can be switched depending on the step (splitting or regeneration). The reactor submodel is a single mass block that exchanges energy in convective and radiative processes between the ambient and the gas inside the reactor and receives all the concentrated solar power from the solar field. The reaction submodel models the energy and the molar balance inside the reactor assuming the reaction rates given in [29]. The sink submodel provide the outlet mass flow rate calculated based on Bernoulli's principle. The solar field and processing plant models

described in [22] were calibrated and validated with experimental data from the Hydrosol facility and the predictions showed good agreement.

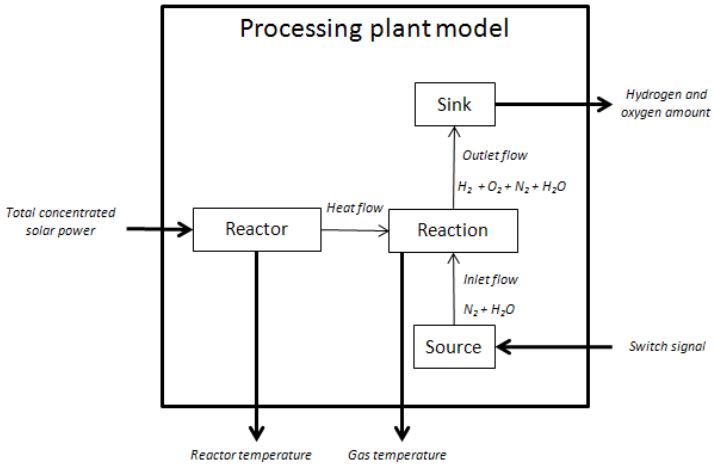

Figure 5: Processing plant model scheme.

Table 2 shows the controller parameters (proportional gain, K_p, and integral time, T_i) adjusted in the simulation and the results using a typical irradiance curve measured in February with a pyrheliometer conected to the acquisition system of Hydrosol (see the top graph of Fig. 6).

Time (HH:MM)	**Step (°C)**	T_{st} **(min)**	**Overshoot (°C)**	K_p $(^oC^{-1})$	T_i **(s)**
09:51	0-1200	25.8	19	0.008	210
10:31	1200-800	11.8	-37	0.04	210
11:01	800-1200	14.4	12	0.023	210
11:31	1200-800	10.4	-41	0.04	210
12:01	800-1200	14.3	9	0.023	210

Table 2: Main results of simulation with the automatic control.

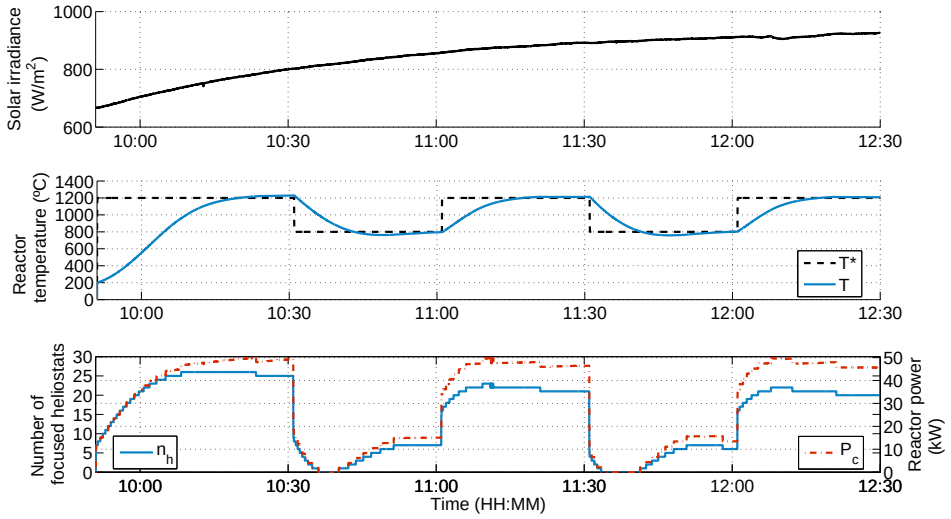

Figure 6: Simulation control results in one reactor using the model described in [22].

Three different tunings are used to carry out a typical Hydrosol experiment. The first one, during start-up where the aim is to reach 1200℃, must be the more conservative because the system starts up at a low temperature and the temperature gradient is steep. Moreover, as pointed out above, the temperature may not exceed 1250℃. Therefore, the PI parameters used are K_p=0.008^{o}C^{-1} and T_i=210 s. Faster tuning is used to reach the production temperature (800℃) for two reasons. First, because of the high thermal inertia which makes it difficult to cool down the system, and second, because the temperature constraints are not as strong as at higher temperatures.

Therefore, the proportional gain is changed (K_p=0.04^{o}C^{-1}). The last tuning for reaching the regeneration temperature is again conservative to avoid high temperature overshoots, but is more aggressive than during start-up (K_p=0.023^{o}C^{-1}).

The result is plotted in Fig 6. The reactor temperature is maintained quite well at the two desired references by changing the number of heliostats focused on the target. The model used [22] estimates the thermal power that reaches the receiver, P_c. About 50 kW is needed to keep the temperature at 1200℃ and 20 kW at 800℃, but the number of heliostats required depends on the irradiance and the time, which affect the incident angle and the solar-field optical-concentration errors. For example, at time 10:30, the number of heliostats focused is n_h=26, whereas at time 12:30 s, n_h=22 because the irradiance and incident angle have changed.

5.2. Real control results

The proposed control system was tested in the Hydrosol facility described in Section 2. It was implemented in MATLAB® and integrated in a LabVIEW® interface which is connected to the main SCADA (Supervisory Control And Data Acquisition) system by means of an OPC server.

An experiment performed in January, 2012 is shown in Fig. 7. The test starts with a mean reactor temperature of 11℃ and a direct irradiance over 750 W/m^2.

The first setpoint step to 1200℃ was at 9:53. At this point, the controller started to increase the number of heliostats that must be focusing on the reactor target to reach the desired temperature. After 26 minutes, the mean reactor temperature reached 1140℃. A new reference step of 800℃ at 10:31

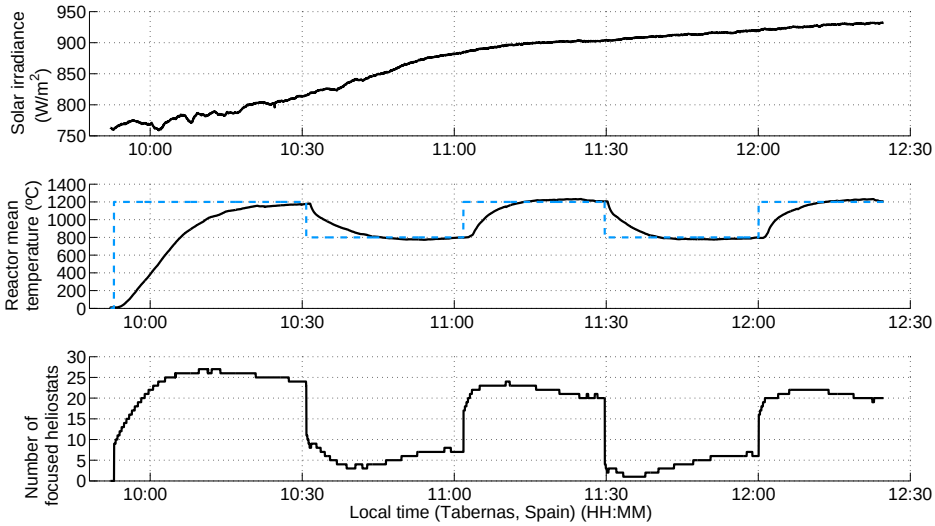

Figure 7: Test with automatic control in the Hydrosol facility.

caused some heliostats to start to go out of focus.Under steady-state temperature conditions, the number of heliostats focused was reduced to fewer than 10. Since the setpoint switches in around 30-minute, at 11.05 a positive step of 400℃ was made. Although controller tuning in this step is more conservative than the previous one and control action slowed down, the settling time was shorter because of system inertia. Two more setpoint changes were made before the experiment was over. Table 3 summarizes the tuning parameters and control measurements. It is important to mention that the tuning parameters differed slightly from those found in the simulation. This is because of model simplifications, mainly in the solar eld, which assumes a constant overall error parameter in the heliostats.

Local time (HH:MM)	**Step (°C)**	T_{st} **(min)**	**Overshoot (°C)**	K_p $(^oC^{-1})$	T_i **(s)**
9:53	0-1200	26.1	-	0.008	110
10:31	1200-800	11.4	-24	0.04	110
11:03	800-1200	9	30	0.023	110
11:30	1200-800	9	-23	0.04	110
12:01	800-1200	9.6	32	0.023	110

Table 3: Main results of the automatic control test in the Hydrosol facility.

As shown in Table 3, using the automatic control for one reactor, the settling time, T_{st}, was kept between 9 and 11 minutes, and overshoots were almost constant at every temperature. This is a great advantage over the results with manual control for both reactors shown in Table 1.

6. Conclusions

In this paper, an adaptive control strategy for controlling the mean temperature in a solar hydrogen reactor was proposed and implemented. Since system thermal inertia is higher during heating than cooling, and the system constraints are stricter at 1200°C, PI control tunings are different. Moreover, the switching procedure ensures continuity in the controller output signal between switches.

The controller was tested in simulations which provided a first tuning estimate. Finally, real experiments were performed in the Hydrosol facility with very promising results.

Future work will reduce the switching time by using feedforward compensations and improving the solar eld model. Moreover, different heliostat selection algorithms will be tested.

Acknowledgements

The authors would like to thank the European Commission for co-funding this work under the HYDROSOL-3D Project "Scale Up of Thermochemical Hydrogen Production in a Solar Monolithic Reactor: a 3^{rd} Generation Design Study (Call GCH-JU-2008-1, Activity SP1-JTI-FCH-2.3: Water decomposition with solar heat sources, Project Number 2425224). The authors would also like to thank the CIEMAT Research Centre and the Spanish Ministry of Science and Innovation for funding Project DPI2010-21589-C05-02.

References

[1] Hoffman, P.. Hydrogen–the optimum chemical fuel. Appl Energ 1994;47(2-3):183–199.

[2] Dincer, I., Zamfirescu, C.. Sustainable hydrogen production options and the role of IAHE. Int J Hydrogen Energ 2012;doi: 10.1016/j.ijhydene.2012.02.133.

[3] Steinfeld, A.. Solar thermochemical production of hydrogen–a review. Sol Energy 2005;78:603 – 615.

[4] Pregger, T., Graf, D., Krewitt, W., Sattler, C., Roeb, M., Möller, S.. Prospects of solar thermal hydrogen production processes. Int J Hydrogen Energy 2009;34:4256 – 4267.

[5] Kodama, T., Gokon, N.. Thermochemical cycles for high-temperature solar hydrogen production. Chem Rev 2007;107(10):4048–4077.

[6] Agrafiotis, C., Pagkoura, C., Zygogianni, A., Karagiannakis, G., Kostoglou, M., Konstandopoulos, A.. Hydrogen production via solar-aided water splitting thermochemical cycles: Combustion synthesis and preliminary evaluation of spinel redox-pair materials. Int J Hydrogen Energ 2012;.

[7] Thomey, D., de Oliveira, L., Säck, J., Roeb, M., Sattler, C.. Development and test of a solar reactor for decomposition of sulphuric acid in thermochemical hydrogen production. Int J Hydrogen Energ 2012;doi: 10.1016/j.ijhydene.2012.02.136.

[8] Hong, H., Liu, Q., Jin, H.. Operational performance of the development of a 15kw parabolic trough mid-temperature solar receiver/reactor for hydrogen production. Appl Energ 2012;90:137–141.

[9] Bulfin, B., Murphy, B., Lübben, O., Krasnikov, S., Shvets, I.. Finite element method simulations of heat flow in fixed bed solar water splitting redox reactors. Int J Hydrogen Energ 2012;doi: doi:10.1016/j.ijhydene.2012.03.163.

[10] Xu, R., Wiesner, T.. Dynamic model of a solar thermochemical water-splitting reactor with integrated energy collection and storage. Int J Hydrogen Energ 2012;37:2210–2223.

[11] Xiao, L., Wu, S., Li, Y.. Advances in solar hydrogen production via two-step water-splitting thermochemical cycles based on metal redox reactions. Renew Energ 2012;41:1–12.

[12] Petrasch, J., Osch, P., Steinfeld, A.. Dynamics and control of solar thermochemical reactors. Chem Eng J 2009;145(3):362–370.

[13] Säck, J.P., Roeb, M., Sattler, C., Pitz-Paal, R., Heinzel, A.. Development of a system model for a hydrogen production process on a solar tower. Sol Energy 2012;86(1):99–111.

[14] Roeb, M., Neises, M., Säck, J., Rietbrock, P., Monnerie, N., Dersch, J., et al. Operational strategy of a two-step thermochemical process for solar hydrogen production. Int J Hydrogen Energy 2009;34:4537–4545.

[15] Camacho, E., Rubio, F., Berenguel, M., Valenzuela, L.. A survey on control schemes for distributed solar collector fields. part ii: Advanced control approaches. Sol Energy 2007;81:1252–1272.

[16] Roeb, M., Säck, J.P., Rietbrock, P., Prahl, C., Schreiber, H., Neises, M., et al. Test operation of a 100kW pilot plant for solar hydrogen production from water on a solar tower. Sol Energy 2011;85:634 – 644.

[17] Camacho, E., Berenguel, M., Alvarado, I., Limon, D.. Control of solar power systems: a survey. In: Proceedings of the 9th International Symposium on Dynamics and Control of Process Systems (DYCOPS 2010). 2010,.

[18] García-Martín, F., Berenguel, M., Valverde, A., Camacho, E.. Heuristic knowledge-based heliostat field control for the optimization of the temperature distribution in a volumetric receiver. Sol Energy 1999;66(5):355–369.

[19] Berenguel, M., Rubio, F., Valverde, A., Lara, P., Arahal, M., Camacho, E., et al. An artificial vision-based control system for automatic heliostat positioning offset correction in a central receiver solar power plant. Sol Energy 2004;76(5):563–575.

[20] Garcia, P., Ferriere, A., Bezian, J.. Codes for solar flux calculation dedicated to central receiver system applications: A comparative review. Sol Energy 2008;82:189–197.

[21] Belhomme, B., Pitz-Paal, R., Schwarzbözl, P., Ulmer, S.. A new fast ray tracing tool for high-precision simulation of heliostat fields. J Sol Energ- T ASME 2009;131:031002.

[22] de la Calle, A., Roca, L., Yebra, L., Dormido, S.. Modeling of a two-step solar hydrogen production plant. Int J Hydrogen Energ 2012;doi: 10.1016/j.ijhydene.2012.04.056.

[23] Ballestrín, J., Marzo, A.. Solar radiation attenuation in solar tower plants. Sol Energy 2011;86(1):388–382.

[24] Blanco-Muriel, M., Alarcón-Padilla, D., López-Moratalla, T., Lara-Coira, M.. Computing the solar vector. Sol Energy 2001;70:431–441.

[25] De la Calle, A., Roca, L., Yebra, L., Vidal, A.. A simulator tool to test control algorithms in a hydrogen solar plant. In: Proceedings of the SolarPACES 2011. 2011,.

[26] Brdys, M., Tatjewski, P.. Iterative algorithms for multilayer optimizing control. Imperial College Pr; 2005. ISBN 1860945147.

[27] Åström, K.J., Hägglund, T., Hang, C., Ho, W.. Automatic tuning and adaptation for pid controllers-a survey. Control Eng Pract 1993;1(4):699–714.

[28] Åström, K.J., Hägglund, T.. PID controllers: theory, design, and tunning. Instrument Society of America; 1995.

[29] Agrafiotis, C.C., Pagkoura, C., Lorentzou, S., Kostoglou, M., Konstandopoulos, A.G.. Hydrogen production in solar reactors. Catal Today 2007;127:265 – 277.

List of Figures

List of Tables

Name	Description	Units
A	Heliostat mirror area	m^2
c	On-focus indicator	-
$\mathbf{H}$	Array of identifiers	-
I	Direct solar irradiance	$\mathrm{W} \cdot \mathrm{m}^{-2}$
K_p	Proportional gain	$^{\mathrm{o}}\mathrm{C}^{-1}$
n_h	Number of heliostats focused	-
n_t	Heliostats total number	-
$\mathbf{N}_h$	Array of heliostats focused	-
P	Concentrated solar power	W
P_c	Calculated concentrated solar power	W
p_k	k-heliostat solar power concentration	W
$\mathbf{P}^{\xi}$	Arranged vector of solar power contributions	W
T	Mean temperature in one reactor	$^{\mathrm{o}}\mathrm{C}$
T^*	Temperature setpoint in one reactor	$^{\mathrm{o}}\mathrm{C}$
T_i	Integral time	s
T_s	Sample time	s
T_{st}	Settling time	s
t	Target	
$\mathbf{U}$	Position vector	$(\mathrm{m}, \mathrm{m}, \mathrm{m})$
α_i	Angle of incidence	rad
β	Global error parameter	-

γ	Atmospheric attenuation	-
ρ	Density	$\mathrm{Kg} \cdot \mathrm{m}^{-3}$

Table 4: Variables list